Laboratory Observations of Waves in the Vicinity of WEC-Arrays

Merrick C. Haller[#1], Aaron Porter[#], Pukha Lenee-Bluhm[*2], Ken Rhinefrank[*], Erik Hammagren[*], Tuba Özkan-Haller[+3], David Newborn[#]

[#]*School of Civil & Construction Engineering, Oregon State University*
220 Owen Hall, Corvallis, OR 97331 USA
[1]merrick.haller@oregonstate.edu

[*]*Columbia Power Technologies*
Corvallis, OR 97333 USA
[2]p.lenee.bluhm@columbiapwr.com

[+]*College of Oceanic & Atmospheric Sciences, Oregon State University*
Corvallis, OR 97331 USA
[3]ozkan@coas.oregonstate.edu

***Abstract*— In order to better constrain models for simulating the environmental effects of large-scale arrays of Wave Energy Converters (WECs), we have performed laboratory experiments using five 1:33 scale, commercially-designed, point-absorber WECs. Multiple array configurations (1-device, 3-device, and 5-device) were subjected to a wide range of wave conditions—both regular waves and fully-directional sea states. The experimental instrumentation was extensive and included: a large number of wave gages and current meters, a 3D WEC motion tracking system, and stereo video for 3D wave imaging in the near-field of the WEC-arrays. Initial results presented here quantify the degree of wave shadowing induced by the various incident wave conditions and demonstrate the dependence of shadowing on the chosen array configuration. Denser WEC-arrays lead to more shadowing, and frequency and directional spreading in the wave field smoothes the wave height variation and reduces the shadow in the lee of the arrays. The results also show a clear relationship between wave shadowing and device performance, which indicates that wave absorption, not scattering, is the dominant process producing the shadow.**

***Keywords*— wave energy, lab experiments, wave shadowing, environmental effects**

I. Introduction

The ocean deployment of multiple Wave Energy Converters (WECs) in large-scale arrays appears imminent. However, there is a significant gap in our present knowledge of the near-field scattering and potential far-field environmental effects due to WEC-arrays. This gap comes from the lack of observational data. To help fill this data gap, we have performed laboratory experiments using five, moored, point-absorber WECs. These WECs are 1:33 scale models of the commercially-designed "Manta" from Columbia Power Technologies (see Figure 1).

Because WECs partially extract and scatter the incident wave energy, they induce both near-field and far-field effects on the ambient wave field. In the near-field, constructive and destructive interference patterns are generated and will influence device performance within the WEC-array. In the far-field, the wave energy extracted and redirected by the devices generates a wave shadow in the lee of the array. However, at large distances shoreward from the array the wave shadow should decay, as wave energy bleeds into the shadow due to diffraction.

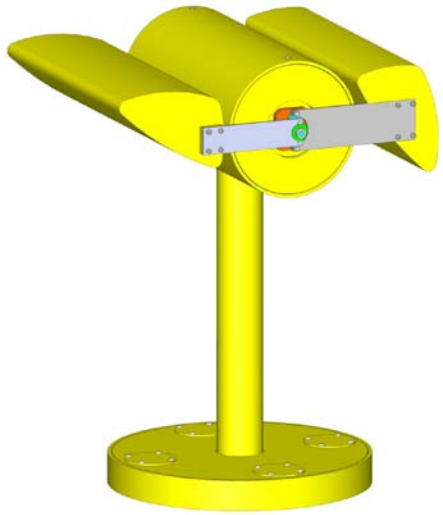

Fig. 1 Illustration of the 1:33 scale "Manta" developed by Columbia Power Technologies.

Assessing the near-field wave effects is important for WEC-array design considerations, and it is important to consider that WEC-array behaviour is not just the linear superposition of individual WEC responses. Instead, there is very likely interplay between individual devices; at the very least, devices in the aft portion of an array will experience shadowing unless the array is very sparse.

Recent efforts that have investigated near-field wave interactions in an array of floating devices were given by Child and Venugopal [1] and Venugopal and Smith [2]. Folley and Whittaker [3] investigated interactions within WEC-arrays in the context of how power capture control affects overall performance in WEC-arrays. Beels et al [4] considered WECs of overtopping-type and allowed for frequency dependent absorption characteristics and investigated the power absorption in a regularly spaced WEC-array versus one arranged in a staggered grid. Beels et al [5] then applied their method directly to a WEC-array made up of "Wave Dragon" devices. Babarit [6] gave quantitative guidance on the area of influence an individual WEC has on other devices in an array. Child and Venugopal [7] and Cruz et al [8] studied the hydrodynamic interactions occurring within arrays and proposed a method for tuning array design to the incident wave conditions. Interference patterns and the degree of wave scattering from individual WECs are also relevant to mooring design [9].

The far-field effects are of interest in order to assess the potential environmental impacts of WEC-arrays. For this assessment we must first quantify the nature and degree of wave shadowing induced by arrays and their overall footprint. For example, if a WEC-array creates additional alongshore variability in wave properties, and this variability extends into the surf zone, this can cause changes in the nearshore circulation patterns and lead to local sediment erosion or accretion.

The recent study of Millar et al [10] investigated changes to the wave field in the lee of a WEC-array with a spectral wave model. Specifically, their work was to address whether the quality of local surfing areas would be diminished by the construction of the "Wave Hub" wave farm off the coast of Cornwall, UK. González-Santamaría et al [11] further developed a wave and current modelling system for the Wave Hub field site in order to investigate some of the baseline hydrodynamic and sediment transport characteristics there, but they did not include the potential effects of WEC-arrays.

Generally speaking, the hydrodynamic modelling of wave propagation processes is highly advanced, i.e. if given accurate incident wave conditions and bathymetry, models can well-simulate local wave conditions and wave-driven currents. Hence, in regards to both the near-field and far-field wave effects, the largest needs are near-field data to verify wave/device interaction models and far-field data to better constrain the WEC-array parameterizations necessary for the large scale hydrodynamic modelling of environmental impact.

Fortunately, unlike other environmental impacts that can only be assessed in the field (e.g. effects on species, such as birds and fishes), we are able to study wave/WEC interactions in the laboratory. This is because the procedures for scaling fluid processes are well-tested and verified and because we have access to fairly large laboratory facilities. The laboratory provides the additional advantage that the incident waves can be controlled, and arrays can be tested over a wide range of possible conditions in a short amount of time.

In Section II we describe the suite of WEC-array experiments we have performed on both the near-field and far-field effects of WEC-arrays. In Section III we present the initial results that demonstrate the wave shadow characteristics of WEC-arrays and the dependence on wave conditions, array configuration, and device performance. The work is summarized in Section IV.

II. Experimental Description

The lab experiments were performed in the Tsunami Wave Basin (TWB) at the Hinsdale Wave Research Laboratory at Oregon State University. The TWB is 48.8 m long, 26.5 m wide, 2.1 m deep, and operates at a maximum water depth of 1.5 m. The wavemaker is comprised of 29 individually-controlled wave paddles of piston-type. The wavemaker is capable of generating normally incident, directional, and multidirectional periodic or irregular waves, as well as solitary or tsunami-like waves.

The WECs used in this project were point-absorbers designed to capture energy both in heave and surge and convert it directly into high-torque rotary motion using direct drive rotary (DDR) generators. Capturing both sources theoretically enables the device to harness twice the energy of point-absorbers operating solely in heave.

As illustrated in Figure 1, the WEC is comprised of three moving bodies: a fore float, an aft float, and spar. The spar is designed to stay relatively stationary in heave by using a large damper at its base. Each float is connected to the top of the spar through a drive shaft. The forward float is connected to the starboard DDR generator and the aft float is connected to the port drive shaft and generator. As the WECs are typically oriented with the fore float heading into the wave, the incoming wave heave and surge force the fore float and aft float to rotate about the spar and drive the generator. At full scale the device diameter is approximately 18 m and its draft from the surface to its lowest point is 25 m.

The available instrumentation for hydrodynamic observations was extensive (see Figure 2). There were 28 in-situ instruments (wave gages plus current meters), which were arranged in instrument arrays designed to resolve the directionally-spread incident wave field, the wave scattering within the WEC-array, and the modified wave field in the lee of the array including the waves that reach the nearshore (far-field) zone.

In order to estimate device performance, a commercial motion tracking system was used to track the three rigid bodies that comprised each WEC using a swarm (~90) of attached LEDs (see Figure 3). These LEDs are tracked with carefully positioned cameras. During wave action, the system of markers and cameras allows the motion of the marked components to be mapped and translated into *x*-*y*-*z* coordinates for motion analysis. The markers/moving bodies exhibit six degrees of freedom – thus rigid body translation in three perpendicular axes combined with rotation about three perpendicular axes (yaw, pitch, and roll).

Generator torque was provided by oil-filled rotary dashpots. Bench testing of each of the dashpots yielded

damping coefficients that characterized the linear torque/speed relationship and allowed torque to be estimated as the product of rotational velocity and individual damping coefficient. Mechanical power was then calculated as the product of rotational velocity and torque. The relative capture width (RCW) was calculated as the arithmetic mean of mechanical power, during the steady state portion of the trial, normalized by the wave energy flux incident through the vertical plane spanning the width of the WEC and extending from the tank floor to the still water level.

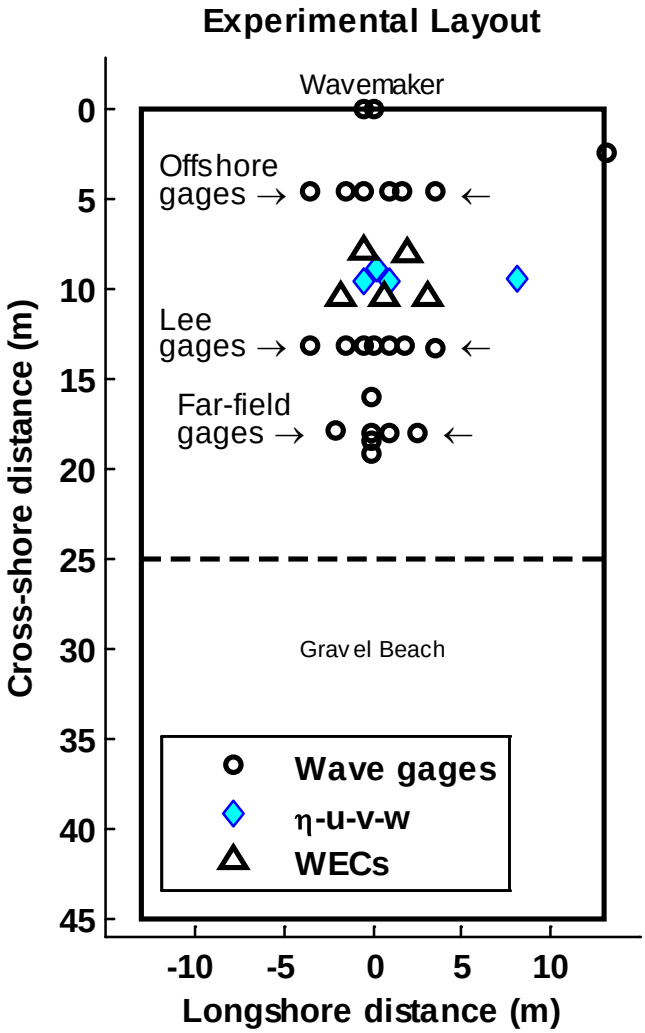

Fig. 2 Layout of in-situ instrumentation.

Finally, a bi-static camera system was installed on the ceiling in order to provide a 3D wave imaging capability through binocular stereo. This capability was directed at analysing the scattered wave field within the WEC-array at high resolution. The constructive and destructive wave interference patterns produced within the array are difficult to resolve with single in-situ gages, but may affect the array performance and the far-field waves. However, these stereo camera data have not yet been analysed.

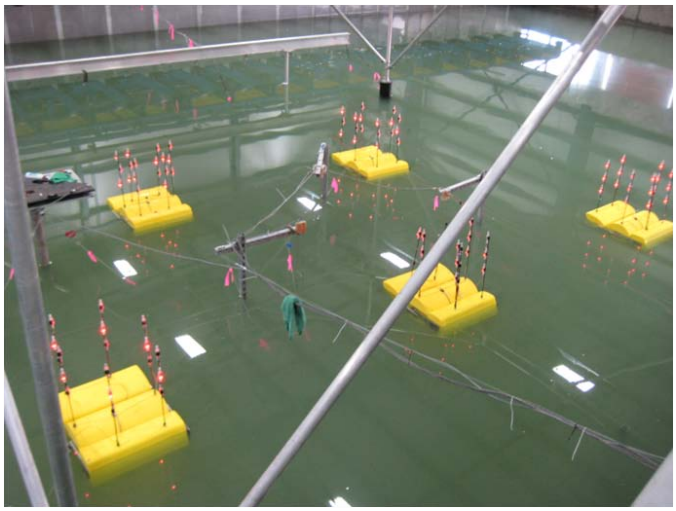

Fig. 3 Photograph of the 5-device WEC-array in a still wave basin. LEDs for motion tracking can be seen attached to the vertical posts on the WECs.

Several different array configurations (single WEC, 3-WEC, and 5-WEC) were subjected to a range of wave conditions—regular waves and directional seas and also variations in the dominant incident wave angle. For real seas cases, the wave frequency spectrum was based on the Pierson-Moskowitz model with a range of different directional spreading factors. Tables I and II list the range of wave conditions and WEC-array configurations that were tested. As shown in Figure 2, a new gravel beach, at 1:10 slope, was placed in the TWB to dissipate wave energy and minimize reflections. The depth of water in the flat portion of the basin was ~1.37 m. When scaled up to prototype conditions, the wave conditions considered span the full range of expected ocean wave conditions for a site on the Oregon coast.

Over the 3-month duration of the experiments, there was variability in the length of data recording for a given trial. The length depended mostly on whether it was regular waves or real seas. For all trials, instrument recording began before the wavemaker was started in order to capture still water and wavemaker ramp-up. However, only the portion of the recorded time series during which waves were fully ramped to the steady-state targeted conditions were used for analysis. For regular wave trials, most analysed time series contained approximately 50 wave periods. For real seas, single WEC-array, waves were run for either 313 or 540 seconds. For real seas, 3-WEC and 5-WEC arrays, waves were run for 540 seconds. After reducing the time series in order to isolate steady-state conditions, typically 90% of the total length was used for analysis.

Most trials were repeated twice, some a third time, in order to quantify repeatability of the wave conditions, WEC-array behaviour, and wave/WEC interactions. In general, incident wave heights, at locations outside of the region of WEC-array influence, showed variability of less than <5% in repeated runs. Closer to the arrays, wave conditions showed more variability with gages within the array showing the highest variability (~0.5 cm).

TABLE I
EXPERIMENTAL CONDITIONS – REGULAR WAVES

H (cm)	Period[1] (s)	Angle[2] (deg)	WEC-array[3]
3	1.0 – 2.8 [11]	0	1
6	0.9 – 2.8 [20]	0, 22.5	1
9	1.0 – 2.8 [11]	0	1
12	1.3 – 2.6 [5]	0	1
6	0.9 – 2.7 [16]	0, 22.5	3, 5
6	1.8 – 2.8 [4]	22.5	3, 5
9	1.0 – 2.6 [7]	0	3, 5
12	1.2 – 2.6 [6]	0	3, 5
15	1.3 – 2.6 [5]	0	1, 3, 5
[1]Wave periods represent max and min of tested range; bracketed number indicates number of periods tested within this range.			
[2]Wave angle ccw with respect to shore normal.			
[3]Number of devices in array.			

TABLE II
EXPERIMENTAL CONDITIONS – REAL SEAS

Wave height	Peak period	Peak direction	Directional Spreading	# of WECs
H_{m0} (cm)	T_p (s)	θ_p (deg)	s[1]	
4.5 7.6 10.6 13.6	1.2, 1.6 1.4, 1.8, 2.2 1.6 2.2	0	4, 10, UD	1
30	2.6	0	UD	1
45.2	2.8	0	2, UD	1
45.2	2.8	22.5	UD	1
4.5 7.6 10.6 13.6	1.2, 1.6 1.4, 1.8, 2.2 1.6 2.2	0	2, 4, 10, UD	3
4.5 7.6 10.6 13.6	1.2, 1.6 1.4, 1.8, 2.2 1.6 2.2	22.5	UD	1, 3, 5
4.5	1.2	0	2, 4, 10, UD	5
4.5 7.6	1.6 1.4	0	4, 10, UD	5
7.6	1.8	0	2, 4, 10, UD	5
7.6	2.2	0	2, 4, 10	5
10.6	1.6	0	2, 4, 10, UD	5
13.6	2.2	0	UD	5
[1]Directional spread parameter, s, for distribution $[0.5*\cos(\theta-\theta_{mean})]^{2s}$, UD is uni-directional (no spreading)				

III. RESULTS

In comparison to real seas, the shadowing induced under regular wave conditions is expected to be the most significant, as previous work, e.g [4], has shown that wave directional spreading acts constructively to smooth out the shadow. Figure 4 shows the distribution of relative wave heights and the wave shadow as observed in the lee of three different WEC-array configurations. The incident regular wave condition for each array configuration was H=6cm, T=1.4 s, and the wave angle was normally incident to the shoreline. Since repeat trials were available for each condition, the data from two trials each were averaged. The figure shows the WEC locations as well, these were determined from the average positions as captured from the motion tracking data. The wave height contours have all been normalized by the mean incident wave height, as measured across the offshore gage array (see Figure 2) for each trial. Hence, the average value across the offshore array is one. This relative wave height parameter is sometimes referred to as the "disturbance coefficient".

From figure 4 it is evident that the wave shadow deepens and spreads laterally as more WECs are added to the array. The larger lateral spread of the shadow also causes the shadow to extend further in the downwave direction. From initial analysis of other trials with H=3, 9, 12, and 15 cm (not shown here) the degree of shadowing does not appear dependent on incident wave height. This suggests that nonlinearity is not influencing these results.

However, we would note that the scattered wave field is more variable in space and time for regular waves when T≤1.3 sec. We have yet to determine the nature and source of this variability, although it is clearly associated with either WEC/mooring interactions or wave/WEC interactions as it is not prevalent outside of the region of WEC-array influence. Further observations of the dependence of WEC-array behaviour on wave period will be given later in the discussion of figures 7-8.

Directional spreading in the incident wave field is expected to smooth out the wave height variations induced by the array. In addition, directional spreading is well known to reduce the degree of shadowing induced by any sort of obstacle, whether it is designed to reflect or absorb.

Figure 5 shows the results from similar wave conditions to figure 4, except that the incident wave field contains frequency- and directional- spreading. For these real seas trials it is appropriate to utilize the significant wave height calculated in the spectral domain. The significant wave height is defined as:

$$H_{m0} = 4\sqrt{m_0}, \quad (1)$$

where m_0 is the zeroth moment of the spectrum. Likewise, we use a spectral measure of wave period defined as the period that contains the highest power spectral density, T_p. Here, m_0 is calculated by integrating the spectrum between $0.5/T_p$ and 5 Hz. Since the real seas trials were much longer duration (time series were ~150-500 x T_p), less repeated trials were made. For the cases shown here, wave heights were not averaged across trials.

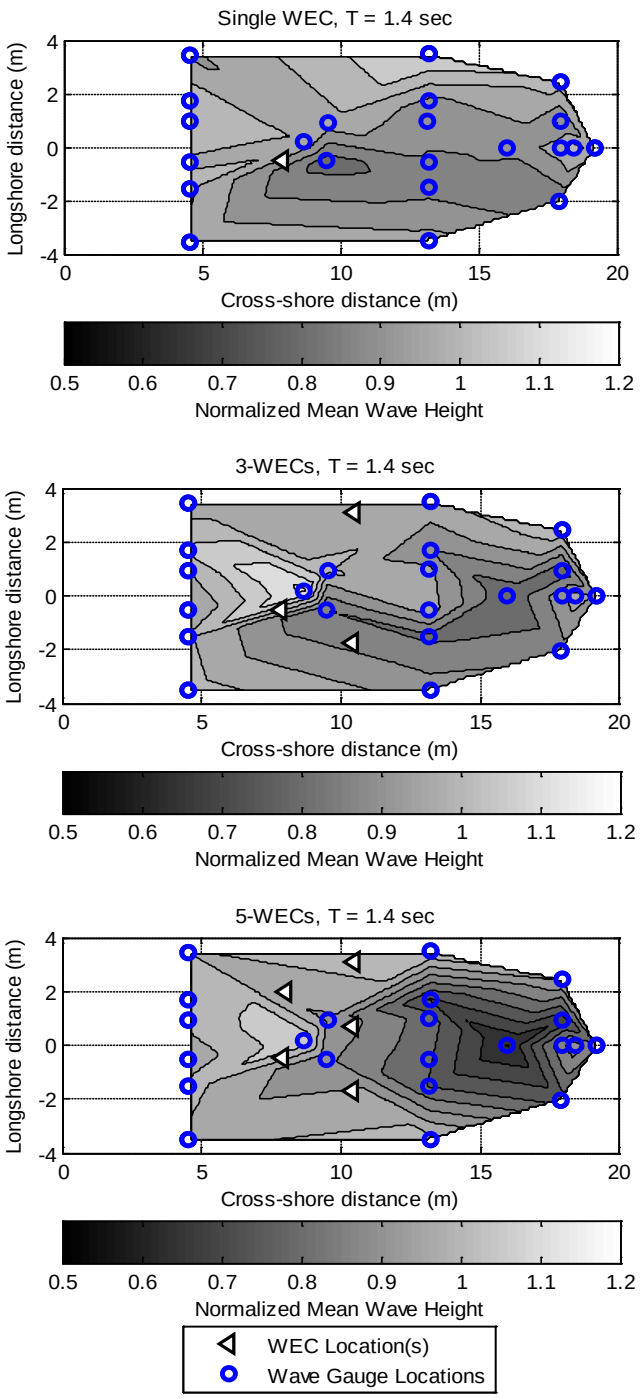

Fig. 4 Relative wave heights measured across the domain for 1/3/5-WEC array (top), (middle), and (bottom), respectively. Regular waves were normally incident, T=1.4 sec. Contour interval is 0.05 and contours were interpolated between measurements.

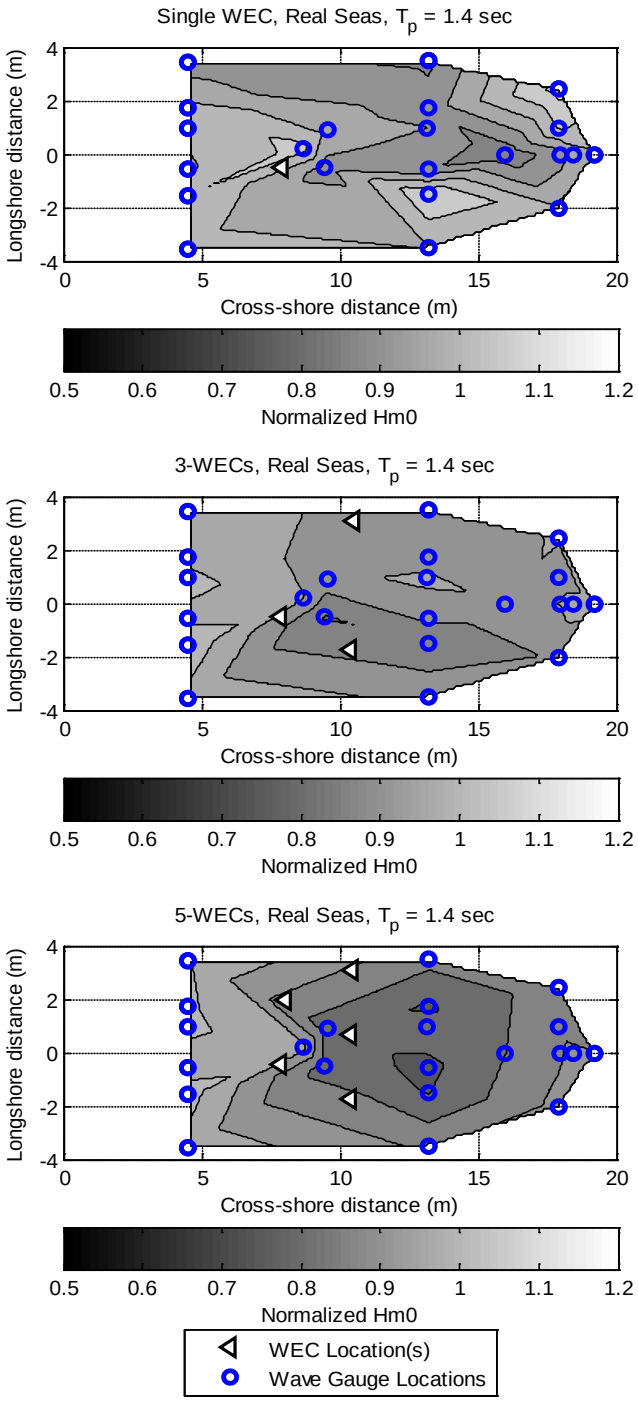

Fig. 5 Spectrally-determined relative wave heights, H_{m0}, measured across the domain for 1/3/5-WEC array (top), (middle), and (bottom), respectively. Real seas, T_p=1.4 sec, peak incidence angle is shore normal, directional spreading factor s=4. Contour interval is 0.05 and contours were interpolated between measurements.

The smoothing effect of spreading is well-illustrated by comparing the regular wave cases in Figure 4 (H=6cm, T=1.4 sec, normal incidence) with their real seas equivalents (H_{m0}=7.58 cm, T_p=1.4 sec, s=4, peak angle normal incidence)

in figure 5. For the real seas cases, the wave height contours are clearly smoothed and there is somewhat less shadowing in the lee of the arrays. For example, the minimum relative wave height in the regular wave, 5-device configuration is approximately 65% versus 80% for the directionally spread case.

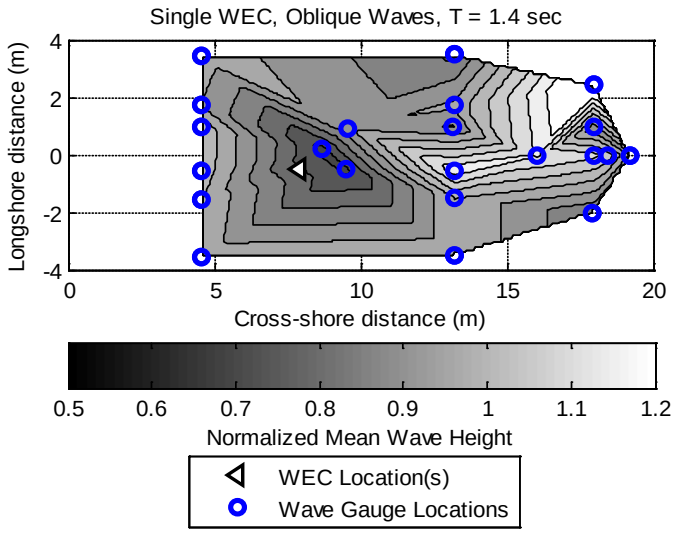

Fig. 6 Relative wave heights measured across the domain for 1-WEC array, oblique incidence (22.5 deg), T=1.4 sec. Contour interval is 0.05 and contours were interpolated between measurements.

The effect of oblique wave incidence was also examined. Figure 6 shows the equivalent of figure 4 (top panel, single device configuration), but with regular waves obliquely incident at 22.5 degrees counter-clockwise from shore normal. The shadow at oblique incidence is qualitatively similar but rotated counter-clockwise to align with the wave direction, as would be expected. At this time the oblique wave incidence cases for the larger WEC-arrays have not yet been analysed. However, we might expect that for multiple device arrays the wave shadow is not simply rotated by oblique incidence. With more devices in the array, oblique incidence essentially changes the device spacing and orientation; hence, we may see more complex changes to the wave shadow.

Figure 7 illustrates the dependence of the shadow on incident wave period and WEC-array configuration. These data represent regular wave conditions only. The figure indicates that there is a clear trend with wave period, with shadowing decreasing with increasing wave period, regardless of array configuration. In addition, the shadow is darker for larger WEC-arrays. Note that at wave periods greater than 2 sec the results from different array configurations are indistinguishable from each other as the differences are small and within the range of noise and repeatability variations. Lastly, the shadowing in the far-field is reduced slightly from that observed in the lee as the wave field recovers due to diffraction.

Taken at face value, figure 7 suggests that the devices more effectively absorb or scatter wave energy at shorter periods. Figure 8 suggests that absorption is the main effect. Figure 8 approximates the device relative capture width (RCW) as derived from the motion tracking data. Essentially, the motion capture data from a single device operating in isolation has been translated into an estimated RCW. As this is an approximation and not an absolute measure of energy capture, the absolute values are still proprietary and not shown. However, the variation with wave period shows a strong correlation with the shadow data in the lee and far-field arrays shown in figure 7.

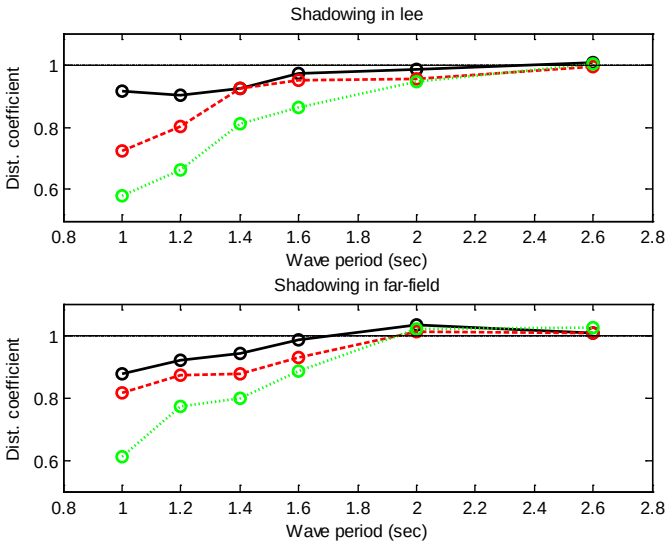

Fig. 7 Relative wave height vs wave period at (top) the lee gage array (±1.5 m from basin centreline) and (bottom) the far-field gage array (±2 m from basin centreline) as a function of WEC-array configuration, 1-device (black/solid), 3-device (red/dashed), and 5-deivce (green/dotted).

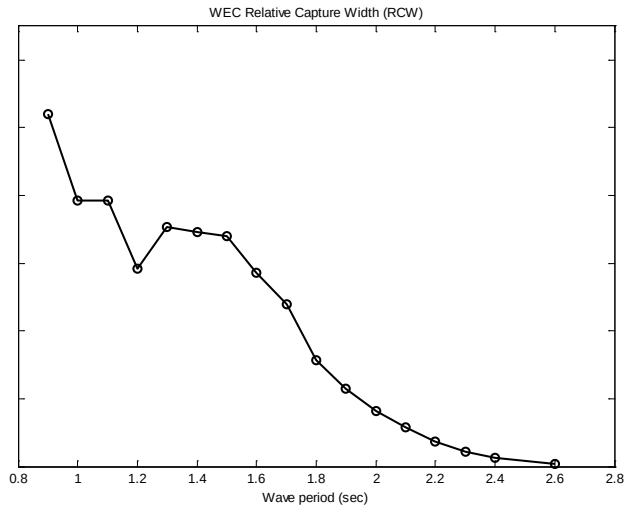

Fig. 8 Relative capture width of a single WEC, measured during 1-device WEC-array tests.

The combined results of figures 7-8 show that the wave shadow increases with the number of devices in the array and decays at periods away from the WEC design condition. In

addition, figure 7 shows that though the wave field has recovered somewhat at the far-field array, at this distance from the WEC-array the wave shadowing is still measurable and significant. Finally, the variation of device performance (approximate RCW) with wave period is well-correlated with the degree of shadowing, which indicates that wave absorption is the dominant process inducing the wave shadow.

IV. Conclusions

We have performed laboratory experiments using five 1:33 scale, point-absorber WECs arranged in multiple array configurations (1-device, 3-device, and 5-device) in order to better quantify wave scattering from WECs and better constrain large-scale hydrodynamic models for environmental impacts from wave energy arrays. In the laboratory the WEC-arrays were subjected to a wide range of wave conditions—both regular waves and fully-directional sea states. The hydrodynamic observations were extensive, but only initial results are provided herein. Initial results quantify the degree of wave shadowing induced by the various incident wave conditions and demonstrate the dependence on the chosen array configuration. Denser WEC-arrays clearly lead to more shadowing and frequency and directional spreading in the wave field smoothes the wave height variation and reduces the shadow in the lee of the arrays. Finally, the motion tracking data was used as a proxy for device performance. These results also show a clear relationship between wave shadowing and device performance, which indicates that wave absorption, not scattering, is the dominant process here.

Future work will investigate the nature of any wave scattering from the devices, and the directional aspects of the wave spectra. In particular, we will examine the video data from the bi-static camera system to see if we can resolve the 3-D water surface in the middle of the WEC-arrays where scattering should be most significant.

These results and our further work will serve to quantify the near/far-field effects as well as to verify and calibrate state-of-the-art numerical models, which are essential to transferring the results to field sites. These results can also be used to adjust wave farm design priorities to address environmental considerations.

Acknowledgment

This research is supported by the U.S. Department of Energy, Sandia National Labs, and Columbia Power Technologies under Research Subagreement NO. 2010-1698, additional support came from Oregon Wave Energy Trust through Award Number OIC-0911-109. We also wish to thank Tim Maddux and the staff of the Hinsdale Wave Research Laboratory for their considerable efforts.

References

[1] B. F. M. Child and V. Venugopal, “Interaction of waves with an array of floating wave energy devices”, *Proc. 7th European Wave and Tidal Energy Conf*., 2007.

[2] V. Venugopal and G. H. Smith, “Wave climate investigation for an array of wave power devices”, *Proc. 7th European Wave and Tidal Energy Conf*., 2007.

[3] M. Folley and T.J.T. Whittaker, “The effect of sub-optimal control and the spectral wave climate on the performance of wave energy converter arrays”, *Appl. Ocean Res*., 31, 260—266, 2009.

[4] C. Beels, P. Troch, G. De Backer, M. Vantorre, and J. De Rouck, “Numerical implementation and sensitivity analysis of a wave energy converter in a time-dependent mild-slope equation model”, *Coast. Eng*., 57, 471—492, 2010.

[5] C. Beels, P. Troch, K. De Visch, J. P. Kofoed, G. De Backer, “Application of the time-dependent mild-slope equations for the simulation of wake effects in the lee of a farm of Wave Dragon wave energy converters”, 35, 1644—1661, 2010.

[6] A. Babarit, “Impact of long separating distances on the energy production of two interacting wave energy converters”, *Ocean Eng*., 37, 718—729, 2010.

[7] B.F.M. Child and V. Venugopal, “Optimal configurations of wave energy device arrays”, *Ocean Eng*., 37, 1402—1417, 2010.

[8] J. Cruz, R. Sykes, P. Siddorn, and R.E. Taylor, “Estimating the loads and energy yield of arrays of wave energy converters under realistic seas”, *IET Renewable Power Generation*, Vol. 4, Iss. 6, pp. 488—497, 2010.

[9] P. C. Vicente, A. F. de O. Falcão, L. M. C. Gato, and P. A. P. Justino, “Dynamics of arrays of floating point-absorber wave energy converters with inter-body and bottom slack-mooring connections”, *Appl. Ocean Res*., 31, 267—281, 2009.

[10] D. L. Millar, H. C. M. Smith, and D. E. Reeve, “Modelling analysis of the sensitivity of shoreline change to a wave farm”, *Ocean Eng*., 34, 884—901, 2007.

[11] R. González-Santamaría, Q. Zou, S. Pan, and R. Padilla-Hernandez, “Modelling wave-tide interactions at a wave farm in the southwest of England”, *Proc. ICCE 2010*, 2010.